Journal of Applied Engineering and Technological Science
Vol 4(1) 2022 : 16-23

FINITE ELEMENT ANALYSIS OF SS316L-BASED FIVE-HOLE PLATE IMPLANT FOR FIBULA RECONSTRUCTION

Nanang Qosim[1]*, Zakki Fuadi Emzain[2], AM. Mufarrih[3], Ratna Monasari[4], Fataa Kusumattaqiin[5], Rangga E. Santoso[6]
Department of Mechanical Engineering, Politeknik Negeri Malang, Indonesia[1,2,3,4]
Department of Chemical Engineering, Politeknik Negeri Samarinda, Indonesia[5]
Department of Energy and Power, Cranfield University, United Kingdom[6]
nanangqsm@polinema.ac.id

Received : 21 May 2022, Revised: 24 July 2022, Accepted : 08 August 2022
*Corresponding Author

ABSTRACT
The design of a product is the first stage that determines its success. In designing an implant product, it is necessary to carefully and carefully consider the strength of the structure, which will determine the implantation process in the bone. This study aims to analyze the design performance of SS316L-based plate implants for fibula restoration. The method used in this study is using a Finite Element Analysis approach. The simulated model design has dimensions of 35 x 5 x 1.5 mm and five holes with a 2-3 configuration. The results of the bending test simulation showed that the values for both displacement and Von Mises stress that occurred (0.008 mm and 116 MPa of each) were still considerably below the yield stress of the SS316L material. The same results were also shown in the tensile test simulation, although the clamping setting on the plate was changed on the other side. From this finite element analysis approach, the SS316L-based five-hole plate implant design has a fairly good strength performance as a fibular bone-implant restoration product.

Keywords: *Plate, Implant, Finite Element Method, Von Mises, Fibula, SS316L*

1. Introduction

A fibular injury is an injury to the bone in the area of the foot between the knee and the sole. Actually, between the knee and the sole, there are two bones, namely the tibia and fibula bones. The tibia is a bone that is at the front or what we call the shinbone. While the fibula bone itself is located on the side of the tibia bone and is smaller (Taberner et al., 2019; Zahn et al., 2012), as shown in Figure 1. The position of these two bones is the longest in the leg, and most susceptible to impact. Hence, it is very susceptible to injury, easy to crack and even the worst part will break (Dursun et al., 2020). In addition to traffic accidents, the most frequent causes of fibular trauma are in sports, especially football (Werner et al., 2017; Zaki et al., 2020).

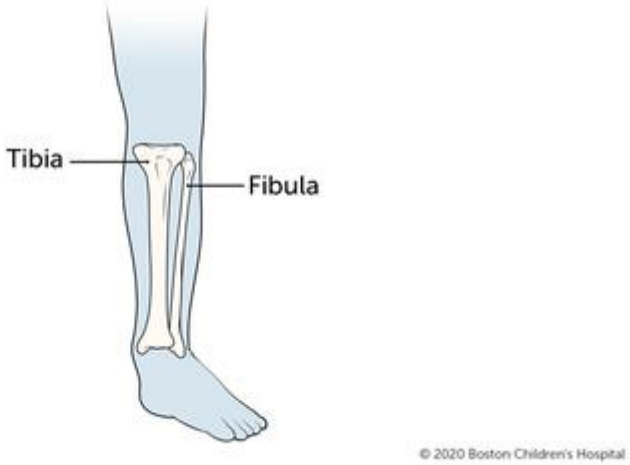

Fig. 1. Tibia and fibula (Boston Children's Hospital, 2020)

For the treatment of trauma to the fibula bone, a plate-shaped implant has several holes depending on the length of the implant. The larger or longer the fracture area, the longer the implant size used. For the installation of the plate, a surgical operation is carried out first. Then the plate will be fixed using screws and left for several months for the healing process before surgical removal of the implant can be performed (Qosim et al., 2018).

Stainless Steel AISI 316L has been widely used as a material for orthopedic implants, dental implants, and cardiovascular stents due to its suitable mechanical properties, workability, high corrosion resistance, chemical stability, and low cost (Godbole et al., 2015; Mojarad Shafiee et al., 2020; Pathote et al., 2022). After Stainless Steel 304/A2, grade 316L Stainless Steel, often known as A4 Stainless Steel or marine grade stainless steel, is the second most prevalent austenitic stainless steel (Dhib et al., 2016). The main alloying elements, after iron, are chromium (16-18%), nickel (10-12%), and molybdenum (2–3%), with small amounts (<1%) of silicon, phosphorus, and sulfur (Dursun et al., 2020; Kong et al., 2020). Due to local corrosive assault by chlorides and widespread corrosion by reducing acids, such as sulfuric acid, the inclusion of molybdenum gives stronger corrosion resistance than 304. Stainless Steel 316L is a low-carbon variant of Grade 316. When cold worked, 316 stainless steel may provide high yields and tensile strengths comparable to Duplex stainless steel (Akinwamide et al., 2022; Ren et al., 2019).

Finite element analysis (FEA) is one of the computational methods that has gained widespread acceptance in the field of orthopedic research (Cao et al., 2019; Emzain et al., 2021). Wong et al., utilized a finite element model of the bony part of the lower leg generated on the basis of computed tomography data from the Visible Human Project. They found that the finite element linear static analysis resulted in relevant fracture localizations and indicated relevant fracture patterns (Wong et al., 2010). Wang et al., used FEA to study the relationship of the tibial tunnel (TT) with fracture patterns and implants (Wang et al., 2021). Lu et al., utilized 3D imaging and FEA of elite fencers for asymptomatic foot and ankle structural injuries (Lu et al., 2022). Thakre et al. performed research on the lower limb of the human body using 3D modeling and FEA of the tibia. The stresses and displacements of the human tibia bone under physiological loading were evaluated using FEA (Pratik S. Thakre, 2021). A study by Koh et al., used a finite element model of High tibial osteotomy (HTO) that was subjected to physiological and surgical loads in the tibia. Their result showed that design optimization was an effective tool for HTO plate design. This information could aid future developments in HTO plate design and could be expanded to other implant designs (Koh et al., 2019).

Computational simulations of biomechanical research can give more information about the stability and usefulness of bone constructions (Huang et al., 2015; Qosim et al., 2020; Steiner et al., 2015). As a result, we used the finite element method to explore the influence of the parameters on the stability of plate fixation on tibial shaft fractures. The goal of this work is to create a patient-specific plate design for post-fracture finger rehabilitation by statistically exploring bending and tensile strength using FEM in line with Indonesian anthropometry. The design has two significant benefits. To begin with, the proper stress distribution of the implant is believed to reduce implant surface wear as well as the likelihood of early loosening. Second, The right strength-to-weight ratio based on the patient's condition will reduce postoperative therapy as well as implantation failure.

2. Research Methods

Computer-Aided Create (CAD) software (CATIA V5R17, *Dassault Systèmes*, French) was used to design the five-hole plate implant. The design produced referenced commercially available components that were then adjusted based on surgeon advice. The model was then simulated using the software using a finite element analysis approach. In this simulation, computations were carried out to determine the displacement value in mm, and the Von Mises stress in N/m^2 unit.

The first step that must be done to perform a finite element simulation was to determine the mesh size or meshing process. Meshing is a continuous process of discretizing into discrete computational domains so that the equations in it can be solved and produce solutions (Berrone et al., 2019). The smaller the counting process, the more accurate the surface area results

obtained (Tavelli & Dumbser, 2016). However, if the enumeration is too much, the resulting equations will be more and more and require a computational process that is too long.

Table 1. Stainless Steel 316L

Parameters	Value
Elements (wt%)	2 Mn; 0.75 Si; 16-18 Cr; 10-14 Ni; 2-3 Mo
Tensile strength (MPa)	485
Yield strength (MPa)	170
Elongation in 50 mm (%)	40
Hardness (Brinell/Rockwell)	217/96

Tensile and bending tests were among the simulated tests used to measure mechanical strength. In this investigation, the load that would ordinarily occur on the fibula was considered to be 100 N and 10 N for tensile and bending load, respectively. The boundary conditions were then considered to be this condition. Stainless Steel 316L was employed in this simulation, and the mechanical parameters are listed in Table 1.

4. Results and Discussions

4.1 Design of Model

The major goal of this five-hole plate implant's design was to provide a firm internal fixation. This was done to ensure a proper fit between the implant and the bone. Figure 2 shows a design solution that incorporates numerous commercial goods as well as surgeon input, a straight, non-locking plate with five holes in the design shape. This model has dimensions of 35x5x1.5 mm. The decision to choose this design was based on the convenience of the manufacturing process if it were to be made into a mass-produced item. Another factor to consider was the plate's positioning, which was believed to avoid translocation when utilized in fracture rehabilitation.

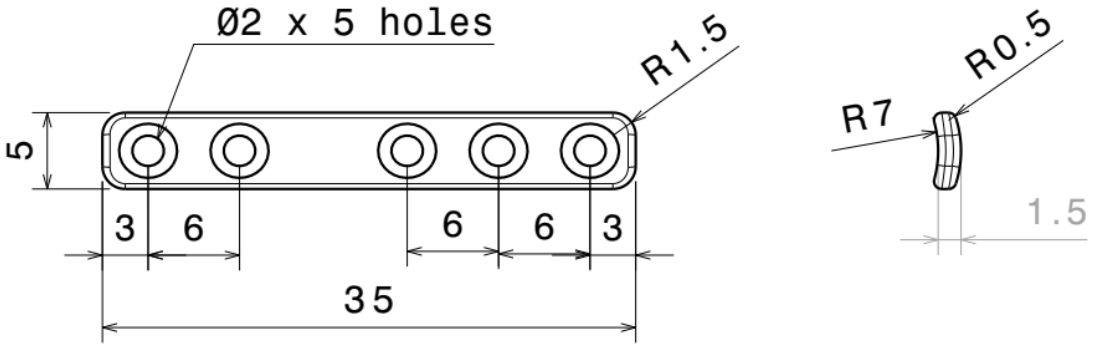

Fig. 2. Technical drawing of five-hole plate implant's design

4.2 Finite Element Analysis Results

Meshing was done automatically in this FEA (finite element analysis) with good quality utilizing a predefined mesh size range in the kind of curvature with 0,1 in size. Figure 3 depicts the meshing result employed in this investigation, which has a total of 122,235 nodes and 563,483 elements.

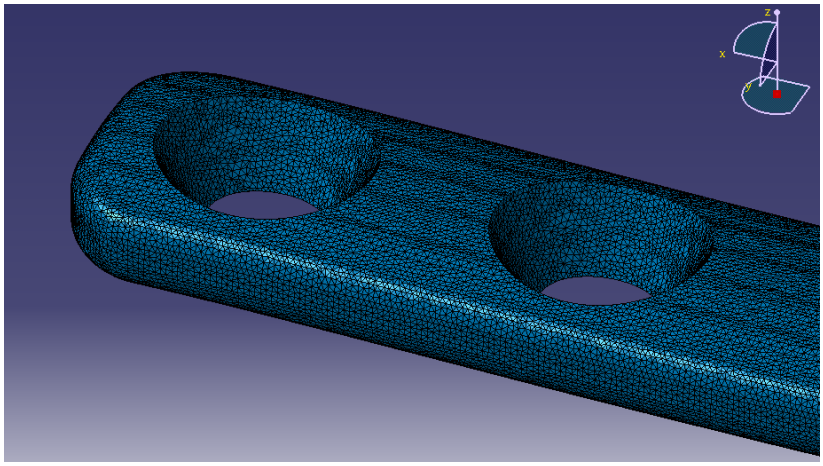

Fig. 3. Discretization of the model

First of all, in the bending test simulation, the compressive load of 10 N was centered right in the middle of the model. The results of The Von Mises stress distribution were depicted in Figure 4 as a consequence of the computation. The stress levels were depicted by hues ranging from red to blue, indicating low to high-stress levels, respectively. The simulation results revealed that the stress was $1.16x10^8$ N/m2 or 116 MPa. The area that experiences the greatest stress was the area around the holes located at the end of the plate side and a hole in the middle of the model. This value was still smaller than the yield value of SS 316L material of 170 MPa. From Figure 4 it was also elucidated that the displacement that occurs was 0.008 mm which was dominantly concentrated in the middle of the model.

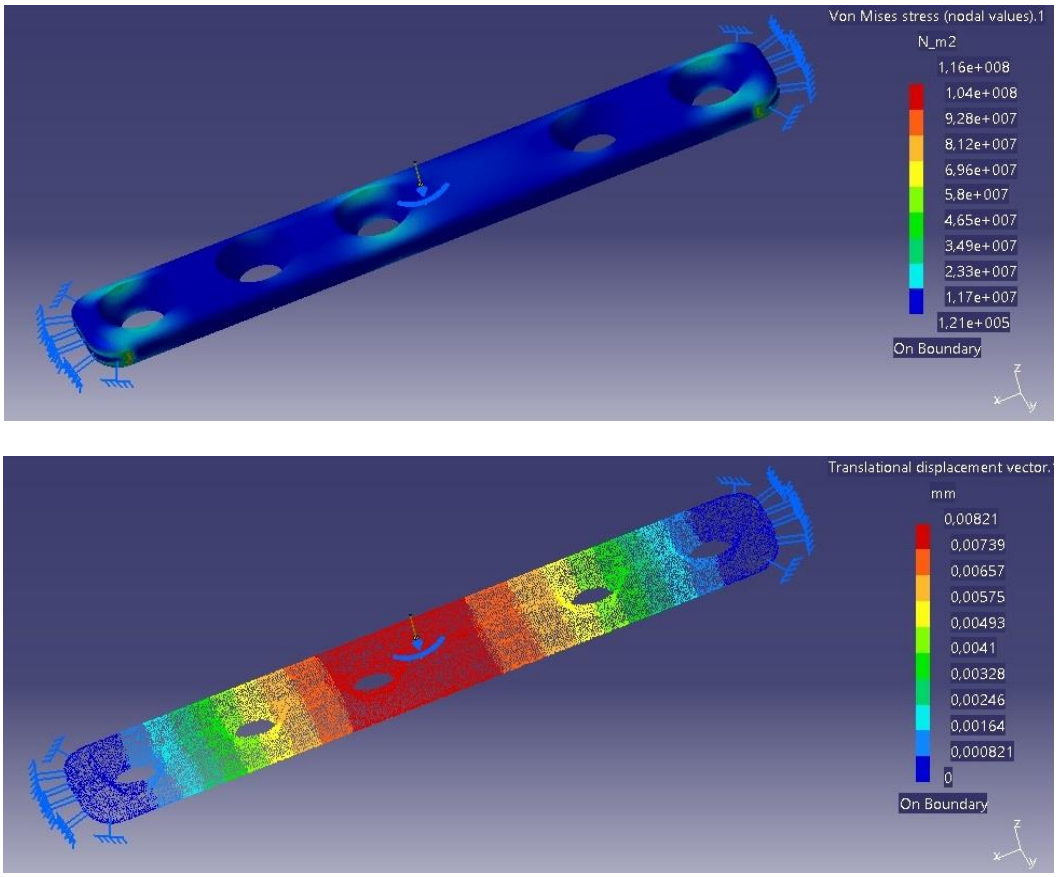

Fig. 4. Simulation Results of The Bending Load

Turning to the other hand, in the tensile test simulation, two kinds of simulations were carried out. The first simulation was to do clamping on the side of the plate which had two holes with the other side being the part that experiences tensile loads. Another simulation was the opposite setting whereas clamping was applied to the side of the plate containing three holes. The results of the bending test simulations for each of these settings were shown in Figures 5 and 6, respectively. Figure 5 depicted that the model with tensile loading on the side containing 2 holes experienced a displacement of 0.039 mm. On the other hand, the displacement that occurred in the model with tensile loading on the side containing 3 holes was 0.057 mm. This value was slightly different from the previous one. However, these two displacement values had similarities which were more concentrated at the end of the model that experienced tensile loads.

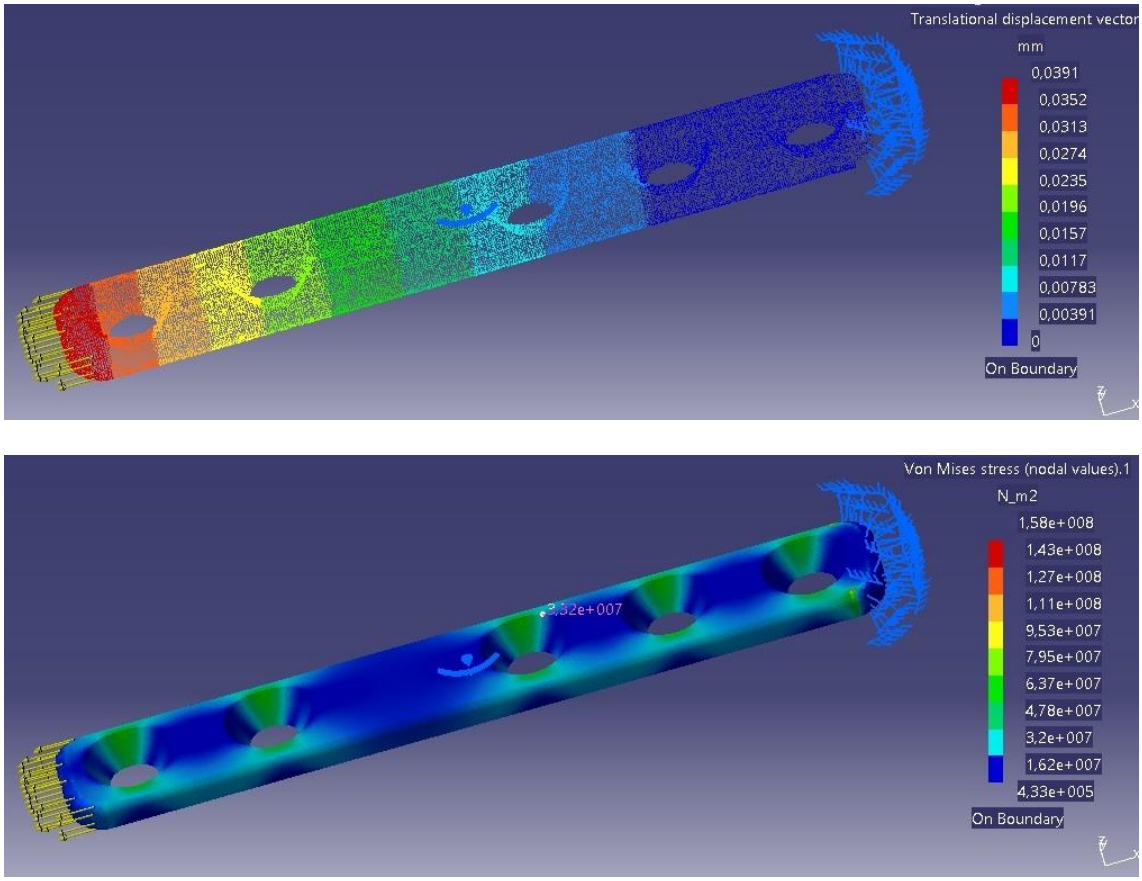

Fig. 5. Simulation Results of The Tensile Load in The Side Containing 2 Holes

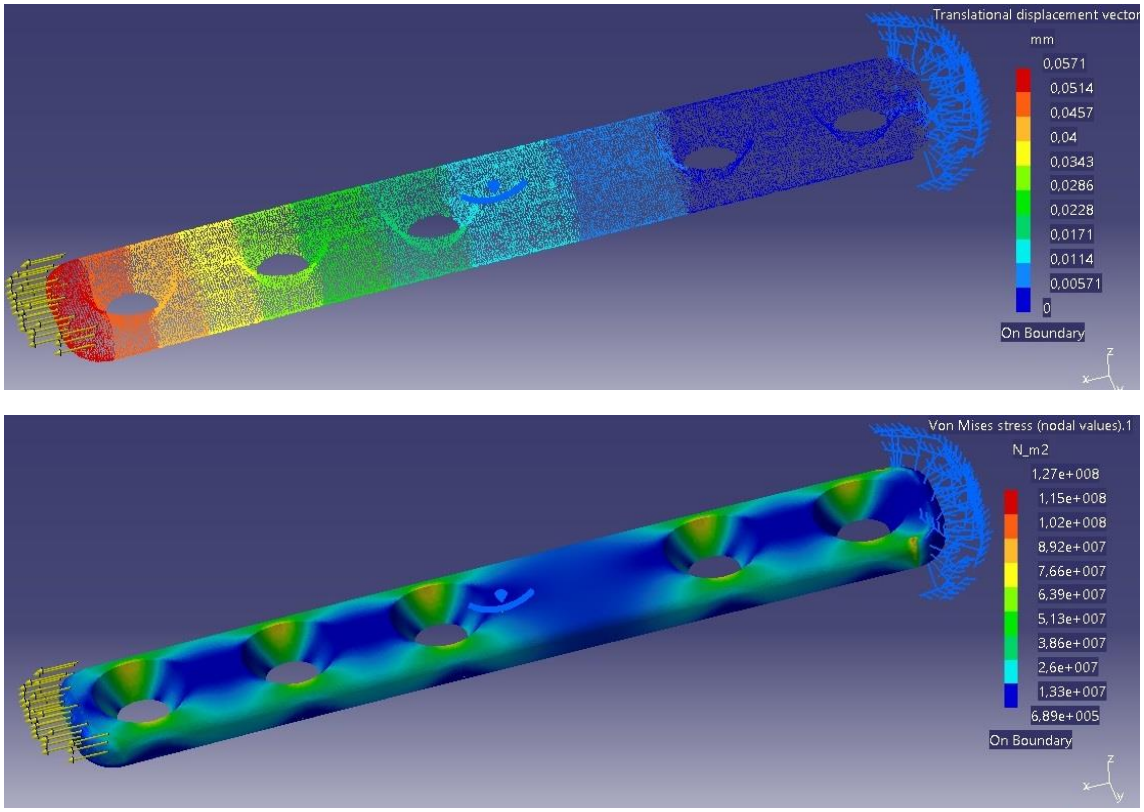

Fig. 6. Simulation Results of The Tensile Load in The Side Containing 3 Holes

The diversification of the location of the loading on the model also affected the value of the resulting Von Mises stress. From Figures 5 and 6, it was revealed that the Von Mises stress values for the model with clamping on the side of the plate containing three holes and two holes were 1.58×10^8 and 1.27×10^8 N/m^2, respectively. The two figures also elucidated that the greatest stresses were concentrated in the area around all holes, especially on the right and left sides of the holes. However, these two values were still very far from the tensile stress value of the SS 316L material of 170 MPa, even when compared to the yield stress of 170 MPa.

From the computational results of bending and tensile tests, the resulting displacement and Von Mises stress values were still below the allowable values. So we can conclude, from the finite element analysis approach, that this design has a fairly good strength performance.

5. Conclusion

The design and numerical analysis of a five-hole plate implant made of stainless steel 316L for fibula repair were well conducted. FEA findings indicated unequal Von Mises stress and strain distribution after adding a static load to the model. Despite the fact that the stress values were much lower than the yield stress of Stainless Steel 316L, the crucial concentration of stresses was found in the middle of the model. The displacements were also quite small, thus they were not thought to have an impact on performance.

6. Acknowledgement

This research was funded in part by a P2M Politeknik Negeri Malang research grant with the number SP. DIPA-023.18.2.677606/2022.

References

Akinwamide, S. O., Venter, A., Akinribide, O. J., Babalola, B. J., Andrews, A., & Olubambi, P. A. (2022). Residual stress impact on corrosion behaviour of hot and cold worked 2205 duplex stainless steel: A study by X-ray diffraction analysis. *Engineering Failure Analysis, 131*, 105913. https://doi.org/10.1016/j.engfailanal.2021.105913

Berrone, S., Scialò, S., & Vicini, F. (2019). Parallel Meshing, Discretization, and Computation of Flow in Massive Discrete Fracture Networks. *SIAM Journal on Scientific Computing*, *41*(4), C317–C338. https://doi.org/10.1137/18M1228736

Cao, Y., Zhang, Y., Huang, L., & Huang, X. (2019). The impact of plate length, fibula integrity and plate placement on tibial shaft fixation stability: A finite element study. *Journal of Orthopaedic Surgery and Research*, *14*(1), 52. https://doi.org/10.1186/s13018-019-1088-y

Dhib, Z., Guermazi, N., Gaspérini, M., & Haddar, N. (2016). Cladding of low-carbon steel to austenitic stainless steel by hot-roll bonding: Microstructure and mechanical properties before and after welding. *Materials Science and Engineering: A*, *656*, 130–141. https://doi.org/10.1016/j.msea.2015.12.088

Dursun, G., Ibekwe, S., Li, G., Mensah, P., Joshi, G., & Jerro, D. (2020). Influence of laser processing parameters on the surface characteristics of 316L stainless steel manufactured by selective laser melting. *Materials Today: Proceedings*, *26*, 387–393. https://doi.org/10.1016/j.matpr.2019.12.061

Emzain, Z. F., Amrullah, U. S., Mufarrih, A., Qosim, N., & Herlambang, Y. D. (2021). *Design optimization of sleeve finger splint model using Finite Element Analysis*. *19*, 6.

Godbole, N., Yadav, S., Ramachandran, M., & Belemkar, S. (2015). A Review on Surface Treatment of Stainless Steel Orthopedic Implants. *Int J Pharm Sci Rev Res*, *33*, 5.

Huang, X., Zhi, Z., Yu, B., & Chen, F. (2015). Stress and stability of plate-screw fixation and screw fixation in the treatment of Schatzker type IV medial tibial plateau fracture: A comparative finite element study. *Journal of Orthopaedic Surgery and Research*, *10*(1), 182. https://doi.org/10.1186/s13018-015-0325-2

Koh, Y.-G., Lee, J.-A., Lee, H.-Y., Chun, H.-J., Kim, H.-J., & Kang, K.-T. (2019). Design optimization of high tibial osteotomy plates using finite element analysis for improved biomechanical effect. *Journal of Orthopaedic Surgery and Research*, *14*(1), 219. https://doi.org/10.1186/s13018-019-1269-8

Kong, D., Dong, C., Ni, X., Zhang, L., Luo, H., Li, R., Wang, L., Man, C., & Li, X. (2020). The passivity of selective laser melted 316L stainless steel. *Applied Surface Science*, *504*, 144495. https://doi.org/10.1016/j.apsusc.2019.144495

Lu, C., Fan, Y., Yu, G., Chen, H., Sinclair, J., & Fan, Y. (2022). Asymptomatic foot and ankle structural injuries: A 3D imaging and finite element analysis of elite fencers. *BMC Sports Science, Medicine and Rehabilitation*, *14*(1), 50. https://doi.org/10.1186/s13102-022-00444-y

Mojarad Shafiee, B., Torkaman, R., Mahmoudi, M., Emadi, R., Derakhshan, M., Karamian, E., & Tavangarian, F. (2020). Surface Modification of 316L SS Implants by Applying Bioglass/Gelatin/Polycaprolactone Composite Coatings for Biomedical Applications. *Coatings*, *10*(12), 1220. https://doi.org/10.3390/coatings10121220

Pathote, D., Jaiswal, D., Singh, V., & Behera, C. K. (2022). Optimization of electrochemical corrosion behavior of 316L stainless steel as an effective biomaterial for orthopedic applications. *Materials Today: Proceedings*, *57*, 265–269. https://doi.org/10.1016/j.matpr.2022.02.501

Pratik S. Thakre. (2021). Finite element analysis of tibia bone. *International Journal of Biomedical Engineering and Technology*, *35*(4), 318–339. https://doi.org/10.1504/IJBET.2021.114812

Qosim, N., Monasari, R., Emzain, Z. F., Hakim, L., & Sai'in, A. (2020). Finite Element Analysis of Miniplate for Post-Fracture Finger Rehabilitation Device. *Journal of Applied Engineering and Technological Science (JAETS)*, *2*(1), 21–26. https://doi.org/10.37385/jaets.v2i1.160

Qosim, N., Supriadi, S., Whulanza, Y., & Saragih, A. S. (2018). Development Of Ti-6al-4v Based-Miniplate Manufactured By Electrical Discharge Machining As Maxillofacial Implant. *Journal of Fundamental and Applied Sciences*, *10*(3S), 765–775.

Ren, Z., Heuer, A. H., & Ernst, F. (2019). Ultrahigh-strength AISI-316 austenitic stainless steel foils through concentrated interstitial carbon. *Acta Materialia*, *167*, 231–240. https://doi.org/10.1016/j.actamat.2019.01.018

Steiner, J. A., Ferguson, S. J., & van Lenthe, G. H. (2015). Computational analysis of primary implant stability in trabecular bone. *Journal of Biomechanics*, *48*(5), 807–815. https://doi.org/10.1016/j.jbiomech.2014.12.008

Taberner, M., van Dyk, N., Allen, T., Richter, C., Howarth, C., Scott, S., & Cohen, D. D. (2019). Physical preparation and return to sport of the football player with a tibia-fibula fracture: Applying the 'control-chaos continuum.' *BMJ Open Sport & Exercise Medicine*, *5*(1), e000639. https://doi.org/10.1136/bmjsem-2019-000639

Tavelli, M., & Dumbser, M. (2016). A staggered space–time discontinuous Galerkin method for the three-dimensional incompressible Navier–Stokes equations on unstructured tetrahedral meshes. *Journal of Computational Physics*, *319*, 294–323. https://doi.org/10.1016/j.jcp.2016.05.009

Wang, Y., Qi, E., Zhang, X., Xue, L., Wang, L., & Tian, J. (2021). A finite element analysis of relationship between fracture, implant and tibial tunnel. *Scientific Reports*, *11*(1), 1781. https://doi.org/10.1038/s41598-021-81401-6

Werner, B. C., Mack, C., Franke, K., Barnes, R. P., Warren, R. F., & Rodeo, S. A. (2017). Distal Fibula Fractures in National Football League Athletes. *Orthopaedic Journal of Sports Medicine*, *5*(9), 232596711772651. https://doi.org/10.1177/2325967117726515

Wong, C., Mikkelsen, P., Hansen, L. B., Darvann, T., & Gebuhr, P. (2010). Finite element analysis of tibial fractures. *DANISH MEDICAL BULLETIN*, 4.

Zahn, R. K., Frey, S., Jakubietz, R. G., Jakubietz, M. G., Doht, S., Schneider, P., Waschke, J., & Meffert, R. H. (2012). A contoured locking plate for distal fibular fractures in osteoporotic bone: A biomechanical cadaver study. *Injury*, *43*(6), 718–725. https://doi.org/10.1016/j.injury.2011.07.009

Zaki, P., Khakimov, S., Hess, J., & Hennrikus, W. (2020). Femur, Tibia, and Fibula Fractures Secondary to Youth Soccer: A Descriptive Study and Review of the Literature. *Cureus*. https://doi.org/10.7759/cureus.8185